Available online at sjuoz.uoz.edu.krd

journals.uoz.edu.krd

Science Journal of University of Zakho

Vol. 11, No. 2, pp. 139– 152, April-June 2023

p-ISSN: 2663-628X
e-ISSN: 2663-6298

PREPARATION, CHARACTERIZATION AND RELEASING -SWELLING KINETICS OF MYRRH BASED HYDROGEL

Mohammad Ehsan Hamodi*[a], , Mohammed Khalil Younis[a],
[a] Faculty of Science, University of Zakho, Zakho, Kurdistan Region, Iraq - (mohammad.hamodi@staff.uoz.edu.krd.)
Faculty of Science, University of Zakho, Zakho, Kurdistan Region, Iraq - (mohammed.younis@uoz.edu.krd.)

Received: *30 Dec., 2022 /* ***Accepted:*** *01 Feb., 2023 /* ***Published:*** *01 April, 2023* ***https://doi.org/10.25271/sjuoz.2023.11.2.1147***

ABSTRACT:
In this work, Myrrh gum was used with sodium alginate (SA) to create novel Myrrh-Alginate beads composite. These beads were produced utilizing the ionotropic gelation technique. Methylene blue (MB) was employed as a drug model to evaluate the kinetics of drug release and the capacity of the synthesized beads to function as a drug delivery system. The molecular interaction between sodium alginate and myrrh was confirmed by FTIR spectroscopy. The physical characteristics of the Myrrh-Alginate beads, including drug content, particle size, thermal properties, equilibrium water content (EWC), swelling behavior, and equilibrium swelling ratio (ESR), were studied to establish the hydrogel's response type, as well as the releasing kinetics at 37°C and in Phosphate buffer solution (PBS) at pH = 6.8 and 10. All beads (loaded and unloaded) were analyzed by Differential scanning calorimetry, Scanning electron microscopy (SEM) and X-ray diffraction analysis (XRD). The drug content percentages of the Myrrh-Alginate beads increased with a moderate fraction (5%) of Myrrh but dropped with a higher Myrrh percentage. The Myrrh-Alginate beads absorbed more water and swelled more than the pure calcium alginate beads (S2) in pH 6.8 and 10 of (PBS). In a pH 6.8 of (PBS), the Myrrh-Alginate beads demonstrated a controlled and regulated style of releasing and demonstrated a high match with the Korsmeyer-Peppas model as they had the maximum values of the correlation factor (R^2) in this model.

KEYWORDS: hydrogel, drug delivery, Myrrh, swelling, releasing kinetics, methylene blue.

1.INTRODUCTION

Sodium alginate (SA) is a sodium salt of alginic acid, a non-toxic polymer found naturally in coastal brown algae. Typically, alginate has been employed as a tablet gelling agent, thickening agent, and even as a suspending agent in food and pharmaceuticals. It is made up of homopolymeric blocks and blocks having an alternating sequence of uronic acids, -l-guluronic and -d-mannuronic acids [1]. The uronic acids cross-link with divalent cations like Ca^{2+} to form gel. The 'egg-box' structure, which is referred to as the basic mechanism of gelation, is composed of long chain sequences that adopt a regular two-fold structure and dimerize with appropriate chelation of Ca^{2+} [2]. Calcium alginate forms a three-dimensional network due to the nine-co-ordination links formed by each Ca^{2+} ion with an oxygen atom. Alginate beads for drug delivery have been prepared using this phenomenon by dropping SA solution into a calcium chloride solution [3]. Drugs sensitive to stomach acid might be protected from entering the intestine by calcium alginate beads [4,5]. Nonsteroidal anti-inflammatory medicines that produce gastric disorder are thus ideal for drug-loaded alginate beads. The alginate beads might possibly be used to deliver macromolecular medications in a pulsatile fashion in the future [6]. The physical characteristics of calcium-alginate beads may be affected by the addition of certain components. For example, wax particles [7] and magnesium aluminum silicate [8,9] may enhance drug entrapment efficiency and delay drug release from beads by interacting with carboxyl groups of alginates and increasing their hydrophobic properties. Chitin, an insoluble in water polymer, was included into the beads to slow drug release in the pH 6.8 media. This occurred as a result of the creation of a connection between alginate's carboxyl groups and chitin's amino groups [10]. Calcium alginate beads have also been modified with water-soluble polymers such as chondroitin sulfate [11].

The second biological polymer used in presence work was derived from Commiphora Myrrh resin (so called Myrrh). Burseraceae plants of the genus Commiphora exude Myrrh, which is a naturally occurring chemical. It's made up of resins that dissolve in alcohol, oils that are volatile (such as essential oils), and gum that's water soluble [12-14]. Myrrh contains between 30 and 60 percent water-soluble gum. It is mostly constituted of acidic polysaccharides with a 4:1:1 ratio of D-galactose, D-glucuronic acid, and L-arabinose, with roughly 18–20% proteins [15]. In Saudi Arabia, the plant Myrrh is widely utilized. A broad range of medicinal qualities have been documented and used in medicinal herbs to treat a wide range of illnesses, including ulcerative colitis and dermatitis, respiratory infections and dysmenorrhea, amenorrhea and cancers [16,17]. Along with the four fundamental components carbon, hydrogen, nitrogen, and oxygen (which combine to create organic molecules), the Myrrh structure contains numerous inorganic elements. The Myrrh resin contains 62 different elements, several of which are recognized to have biological activities in humans. Calcium and phosphorus are the two most abundant inorganic elements found in the Myrrh extraction, with an estimated total concentration of (183.35ppm), (99.87ppm) respectively [18].

* Corresponding author

2. MATERIALS AND METHODS

2.1. Materials

Sodium alginate (SA), methylene blue (MB) and calcium chloride, was purchased from Sigma Aldrich. Myrrh Gum was bought from local market. Phosphate buffer solutions (PBS) of different pH (6.8, 7.0 and 10) were prepared in the laboratory. All the experiments were conducted in deionized water.

2.2. Bead preparation

Four selected samples (S1, S2, S3, S4) were prepared (figure 1). Sodium alginate took in different (w/v) percentages dissolved in deionized water once pure as in (S1, S2) and as a mixture with certain amount of Myrrh as in (S3, S4) then the previous solutions were dropped via hypodermic syringe into crosslinkers solutions in different ratios and temperatures as illustrated in table (1). The beads were left in those solutions for 24 h, then filtered, and washed several times with deionized water and dried at room temperature for 2-3 days. For loaded beads the model (MB) was added to Sodium alginate solutions with mixing for 2h before crosslinking then the preparation was carried out as mentioned before.

Table 1: Ratios for the produced beads with the different temperatures.

Samples	Alginate (w/v)	Myrrh (w/v)	Crosslinker Myrrh (w/v)	Crosslinker $CaCl_2$ (w/v)	Temperature	Mass of MB (mg)
S1	2.5%	0	5%	0	37ºC	0
S2	1.75%	0	0	1.6%	33ºC	0
S3	1.5%	0.65%	8.5%	0	39ºC	0
S4	1.5%	0.65%	0	1.6%	33ºC	0
SD1	2.5%	0	5%	0	37ºC	5
SD2	1.75%	0	0	1.6%	33ºC	5
SD3	1.5%	0.65%	8.5%	0	39ºC	5
SD4	1.5%	0.65%	0	1.6%	33ºC	5

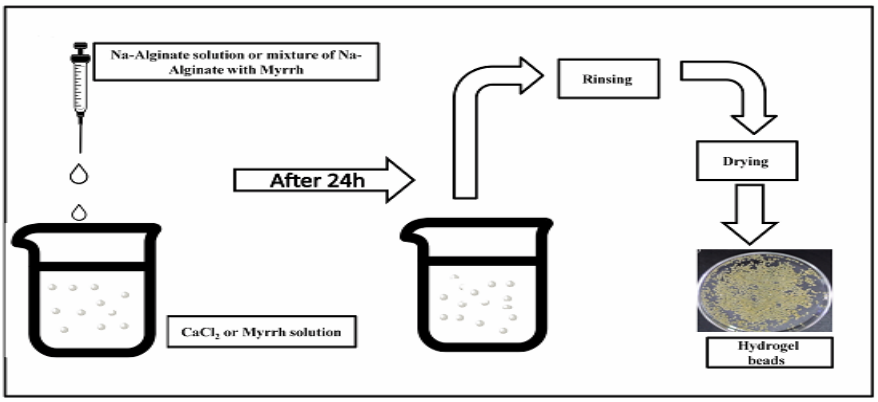

Fig. 1: Schematic preparation for the prepared hydrogel beads composites

2.3. Fourier transformed infrared (FTIR) spectroscopy

FTIR spectra of pure SA, Myrrh and S1, S2, S3, S4 (calcium alginate and Myrrh-alginate beads) and, SD1, SD2, SD3, SD4 (loaded beads) were recorded with FTIR spectrophotometer (Shimadzu FTIR, Kyoto, Japan) using KBr. Each sample was gently thoroughly mixed with KBr powder at a mass ratio of 1:100 and then compressed for 5 minutes at a pressure of 10 tons using a hydrostatic press. The disc was fitted into the sample holder and scanned from 4000 to 450 (cm^{-1}).

2.4. X-ray diffractometry

The X-ray diffraction pattern (XRD) of two selected randomly samples (S3, S4) of synthesized beads was determined using a (XRD-PW1730, Philips, Holland) diffractometer to confirm the type of crosslinking and to measure the crystallinity of the samples using Cu Kα radiation (λ = 1.54060 Å).

2.5. Particle size determination

Particle size of the all-prepared beads in both cases as loaded and pure were determined using a Digital Caliper (Nikon, Japan). Randomly, 10 beads of each sample were sorted and the diameters of each bead were measured and averaged.

2.6. Drug content determination

For 24 hours, weighed loaded beads were immersed and dispersed in 100 ml of pH 6.8 Phosphate buffer. After filtering the solution, the drug content (MB) was determined using a spectrophotometer (Spectrophotometer JENWAY 6300, UK) set to 664 nm. The ratio of the drug to the mass of the hydrogel in the SD_1-SD_4 were calculated.

2.7. Scanning electron microscopic studies

Surface morphology of the prepared beads was characterized before and after loading the drug (methylene blue). Using a scanning electron microscope (SEM), the captured images of the dried beads placed on stubs and then sputter-coated with gold (SEM TESCAN-Vega3, TESCAN, Czech Republic).

2.8. Differential scanning calorimetry (DSC)

A differential scanning calorimeter was used to record the DSC thermograms of Myrrh, SA, Mb, and Myrrh-alginate beads, as well as all samples loaded with beads (SDT Q600 V20.9 Build 20 thermal gravimetric). Each sample (2–4 mg) was precisely weighed and placed in a 40-l aluminum pan without a lid. This was done between 30 and 900 ºC at a rate of 20 ºC / min.

2.9. Swelling Analysis of prepared beads

Phosphate buffer solutions (PBS) were used to conduct swelling studies by incubating dry samples in 10 mL buffer solutions (PBS) at three different pH levels (6.8, 7.0, and 10) and three different temperatures (27 ºC, 37 ºC,47 ºC). Samples were

taken, paper-blotted, and weighed at specified intervals until equilibrium was achieved. Mean values for each pH level were calculated from three swelling measurements.

2.10. Drug Release Experiments

The drug release experiments were conducted using MB as the model drug and Phosphate buffer saline as the release medium (at 37°C and pH 6.8 and 10). We took 4 mL aliquots of the release media and analyzed them with an Agilent Technologies (Spectrophotometer JENWAY 6300, UK) at 664 nm and scheduled times. At the same temperature, the withdrawn release medium was replaced with the same amount of new buffer solution [19]. A standard calibration curve is used to quantify the cumulative quantity of medication released throughout the entire experiment. Each experiment was carried out in triplicate and the mean value was utilized in the evaluation of results. The release constants were calculated using several kinetic models based on the data acquired from drug release. The most used kinetic model is the Korsmeyer–Peppas model [20-24] which employs a semi-empirical equation to examine the kinetic data of the drug released in the early phases (about 60% release) [25]. This model can be stated mathematically as follows:

$M_t / M_f = kt^n$ (i)

where Mt and Mf represent the cumulative quantities of drug released at time t and equilibrium state, respectively; K, the constant combining structural and geometric properties of composite beads; and n, the release exponent, indicative of drug release mechanism. The following are some of the other most widely used kinetic models:

The zero-order Equation (ii):

$M_t / M_f = kt$ (ii)

The first-order Equation (iii):

$\ln (M_t / M_f) = kt$ (iii)

The Higuchi Equation (iv):

$M_t / M_f = kt^{0.5}$ (iv)

The results of the drug release experiment were assessed using different mathematical models, and the model with the greatest correlation coefficient (R^2) was chosen as the best explanation for the drug release process.

3. Results and discussion

3.1. FTIR studies

Figure (2) FTIR spectrum of ordinary calcium alginate bead made by dropping sodium alginate solution into crosslinking agent solution ($CaCl_2$). Stretching vibrations of alginate O–H bonds are identified in the high frequency range of 3000–3600 (cm-1)[26], whereas aliphatic C–H stretching vibrations are recorded at 2935–2810 (cm^{-1}). On the other hand, the bands at 1125 and 767 (cm^{-1}) are assigned to C-O stretching vibrations and C–O stretching vibrations of ring with contribution from C-C, while the bands at 1613 and 1374 (cm^{-1}) are attributed to carboxylate ions. It has been observed in alginate films that the undissociated carboxylic group (C=O) stretches approximately at 1610-1650 (cm^{-1})[27].

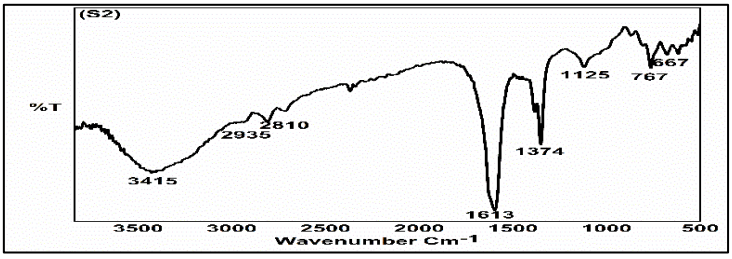

Fig. 2: FTIR spectrum of calcium alginate(S2).

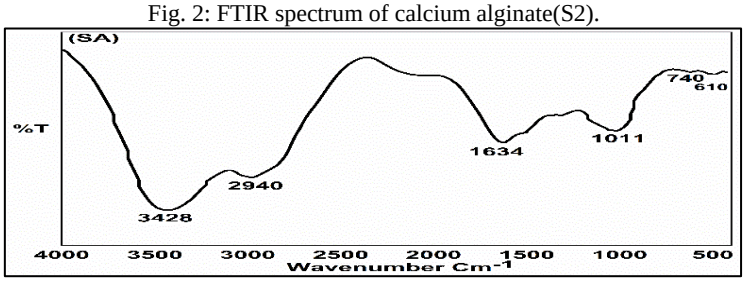

Fig. 3: FTIR spectrum of sodium alginate (SA).

Additionally, the bands at 767 (cm^{-1}) and 667 (cm^{-1}) correspond to mannuronic and guluronic acids, respectively, which are found in the alginate backbone [28,29]. It is critical to observe that the carboxylate ion 1629 (cm^{-1}) asymmetric stretching vibration is shifted to lower wavenumbers than expected for sodium alginate, Figure (3)[5]. This shift might be ascribed not only to the interaction of the usual homopolymeric chain with sodium ions, but also to the change in cation density, radius, and atomic weight caused by the displacement of sodium ion by calcium ion. Calcium alginate beads have a lower absorption surface for O–H stretching vibrations than sodium alginate beads [30]. This modification was most likely brought about by the interaction of the alginate hydroxyl and carboxylate groups with Ca^{2+} during crosslinking.

On Figure (4), the peak values at (3427,2829,1625,1600) (cm^{-1})correspond to the stretching vibrations of O-H and C-H and C=O in the pure Myrrh respectively.

Available online at sjuoz.uoz.edu.krd

Science Journal of University of Zakho

Vol. 11, No. 2, pp. 139– 152, April-June 2023

journals.uoz.edu.krd

p-ISSN: 2663-628X
e-ISSN: 2663-6298

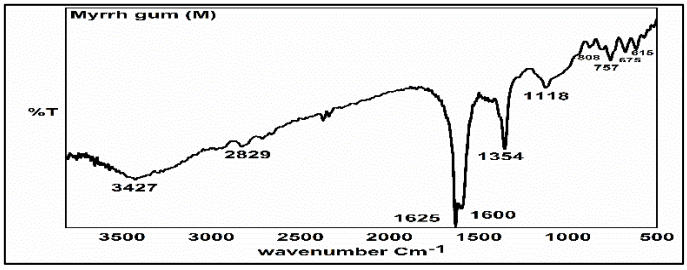

Fig. 4: FTIR spectrum of Myrrh Gum .

FTIR analysis was also used to identify the functional groups of prepared Myrrh-alginate beads. The FTIR spectrum of the new beads before and after MB loading is shown in Figure (5). Alginate beads contain a hydroxyl group (OH group), which corresponds to the peak at 3440 (cm^{-1}). Although this peak reduces to 3431 (cm^{-1}) after MB loading, this indicates that the Myrrh-alginate beads are interacting with the MB through H-bonding interaction. Benhouria et al [31].

When observing the Myrrh-alginate beads chart a peak at 2936 (cm^{-1})that corresponds to the C–H bond's stretching vibration can bee seen. After loading MB into the beads, this peak dropped to 2934 (cm^{-1}). The stretching vibration of the carbonyl (C=O) group peaked at 1635 (cm^{-1}). When MB molecules and alginate beads interact, the peak intensity of the vibration drops and the wavenumber goes down to 1629 (cm^{-1}), which shows the electrostatic interaction between MB molecules and alginate beads [33]. Several earlier studies [32,33] shown the similar behavior for MB adsorption on cellulose-alginate beads. According to the FTIR analysis, alginate beads possess (O-H) and (C=O) functional groups that are categorised as active sites for interaction, allowing for the adsorption of cationic dyes (MB).

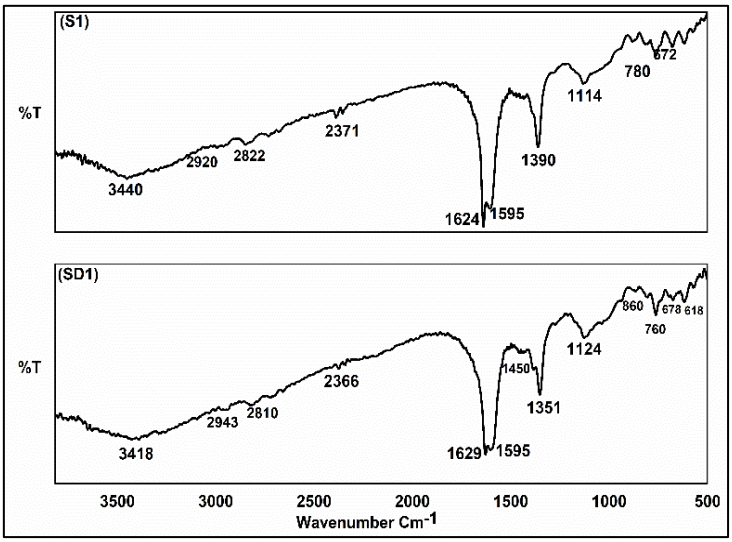

Fig. 5: Myrrh-Alginate beads before (S1) and after (SD1) loading with MB.

3.2. XRD studies

Figure (6) illustrates the XRD pattern of the Myrrh-Alginate beads. The crystal structure can be determined using this technique too [34]. As provide in the figure the existence of amorphous polymer substances in a synthetic bead with a two-peak index and a broad breadth indicates the presence of amorphous polymer substances. There are peaks around 12.5 and 21.5 degrees that are associated with calcium alginate [35]. This suggests that the addition of Myrrh to S4 solution and using Myrrh as crosslinker in S3 had changed the structure of the sodium alginate via Ca-ion crosslinking and produce the new beads. The crystallinity of samples S3 and S4 has been calculated to be 54% and 76%, respectively, which may be attributable to the cross-linking between calcium ions and alginate macromolecules as stated in equation (v)

$$CI = I_{crystalline} / (I_{crystalline} + I_{amorphous}) \quad (V)$$

Where:

CI = degree of crystallinity.

$I_{crystalline}$ = the area of crystalline peaks.

$I_{amorphous}$ = the area of amorphous peaks.

* Corresponding author

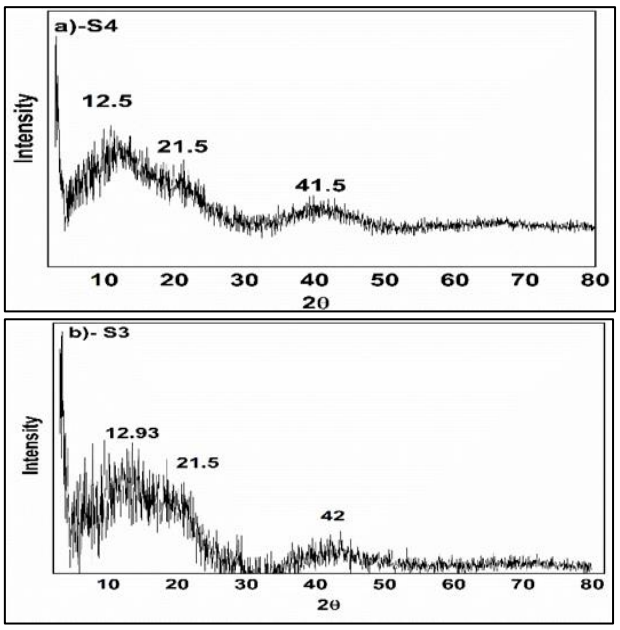

Fig. 6: The XRD chart of a)- S4, b)- S3.

3.3. DSC studies (thermal analysis)

Derivative curves are simply generated from the heat flow curve using a mathematical method and improve in data interpretation. Typically, they may help to determine mathematical parameters and in analyzing data, especially when overlapping peaks are present. For thermogravimetric analysis (TGA) experiments involving weight loss that create a step, the first derivative curve is a valuable tool for investigating stepwise transitions like the glass transition. Second derivatives are simpler to understand than first derivatives when describing a peak. In this situation, the data are flipped, and so any shoulders in the sample signal will settle into independent peaks with in second derivative curves. It is especially helpful for evaluating melting processes and assisting in the identification of shoulders in the peak form caused by several events [36].

Figure (7) shows the DSC thermograms of Myrrh, Na-Alginate, crosslinked beads (S1, S3, S4) of Myrrh-Alg, Methylene blue (MB), and MB-loaded beads. The three produced samples (S1, S3, S4) from Myrrh-Alg composites and Na-Alg showed decomposition temperatures of 209 ^{0}C, 210 ^{0}C, 205 ^{0}C, and 221.5 ^{0}C, respectively. All of these temperatures correlate to the ranges given by Kato [37]. Alginic acid seems to be less stable than that of the salts that have the highest thermal stability. Because the prepared samples had decomposition temperatures that are within the stated range of the Ca-Alginate, we can reasonably assume that the crosslinking occurs as a consequence of the ions displaced by Ca^{2+} in the above-mentioned experimental data.

The endothermic peaks of all three produced samples (S1, S3, and S4) are in the range (288 ^{0}C – 303 ^{0}C), which is between the endothermic peaks of Na-Alg (272.26 ^{0}C) and Myrrh (325.5 ^{0}C). There is an additional endotherm in Na-Alg and S4, while in other samples and in Myrrh, this endotherm disappears, possibly as a result of the lessened Myrrh-Alginate interactions in sample four (S4), figure 7 (a-e).

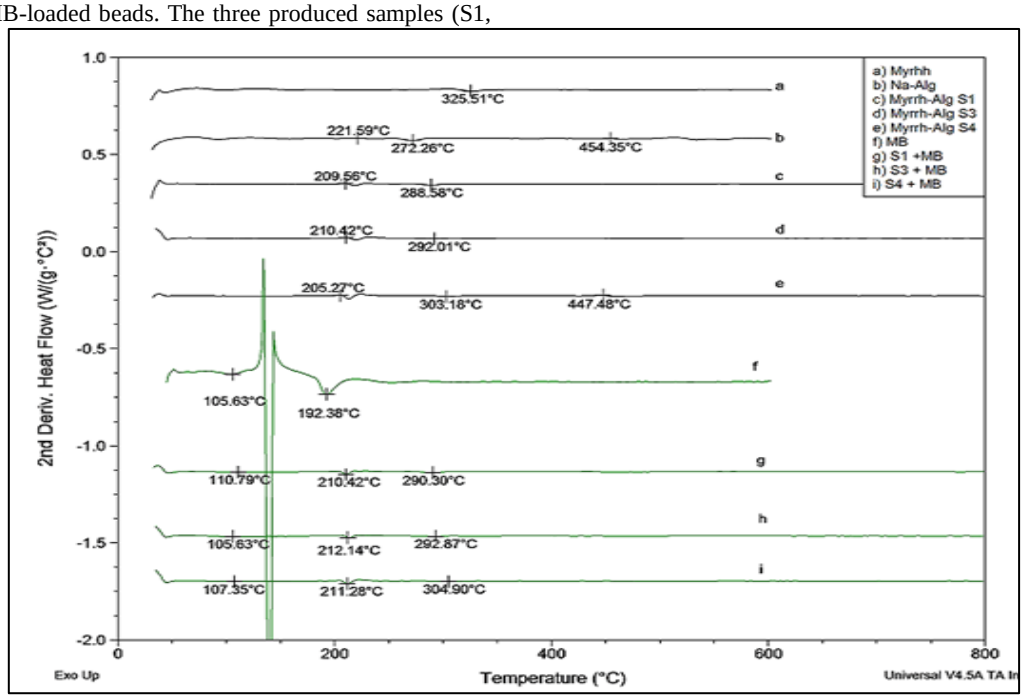

Fig. 7: The second derivative curve DSC of: a) Myrrh, b) Sodium alginate, c) S1, d) S3, e) S4, f) Methylene blue, g) SD1, h) SD3, i) SD4.

Available online at sjuoz.uoz.edu.krd

Science Journal of University of Zakho
Vol. 11, No. 2, pp. 139– 152, April-June 2023

journals.uoz.edu.krd

p-ISSN: 2663-628X
e-ISSN: 2663-6298

Endothermic peaks of MB and Myrrh-alginate beads may be seen on differential thermograms, which reveal the drug state in the beads that have been created. The DSC spectrum of pure MB revealed a prominent melting peak at 139°C, which is much similar to Ali Farmoudeh's reported endothermic peak, figure 7 (f) [38]. Research on the crystalline state of MB indicated the existence of MB in five distinct hydrated forms; consequently, the endotherm may be associated with the solid phase transition of two hydrate forms and the observed exotherm with MB breakdown [39]. When MB was loaded into Myrrh-Alg beads, the differential thermogram of the drug reduced, suggesting that the drug is amorphous; and as provide in figure 7 (g- i) the absence of a distinguishable melting point peak further supports the idea that MB surface adsorption is negligible [38].

3.4. SEM Analysis

SEM examination is utilized to characterize the surface pattern and identify the changes in the surface morphology of the grafted hydrogel beads before and after drug loading and to confirm this process morphologically As illustrated in the figures below Figure 8, dry Myrrh-Alg beads exhibit varied morphological styles on their surfaces, which may be related to the varying ratios of their components, as well as the procedures and temperatures used to prepare them. S1, which is made by dropping pure alginate (2.5%) in Myrrh solution (5%) at 37^0C, demonstrates the smooth and soft surface with holes and caves seen in figure 8 (a). Beads made by dropping pure Alginate (1.75%) into calcium chloride (1.5%) at 33^0C (S2) had a cracked, irregular, and broken surface, figure 8 (b). This could have been caused by dehydration, according to Pasparakis [40].

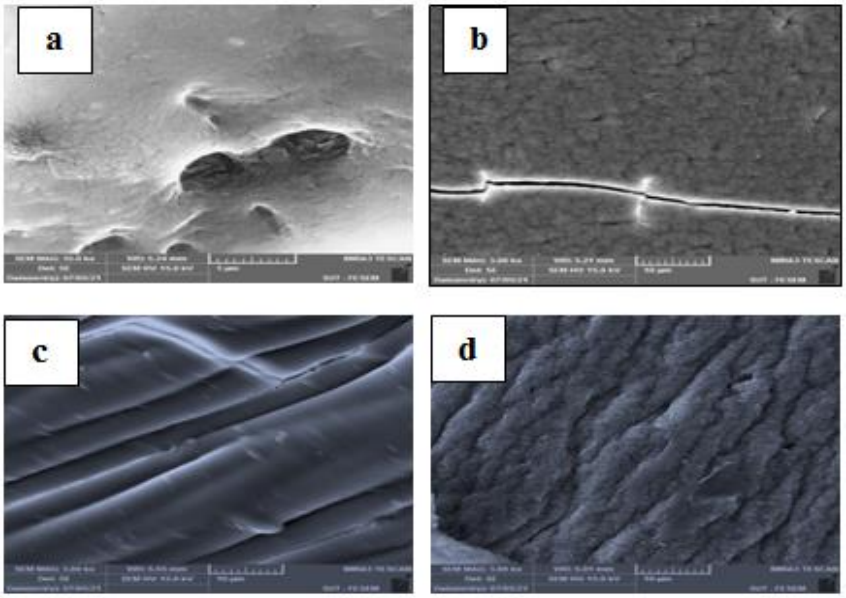

Fig. 8: The SEM images of the four selected Myrrh-Alginate and Calcium Alginate beads: a)- S1, b)-S2, c)- S3, d)- S4.

When Myrrh is present in the core of both S3 and S4, tiny amounts (0.65%) of Myrrh tend to produce more homogeneous and regular surfaces, while both have a bandy and barky pattern as illustrated in figure 8 (c-d). The organization and arrangement of those beads' textures may be attributed to the process of double crosslinking, which occurs from the inner to the outer and vice versa. The degree of crystallinity, as determined by XRD technique, of both S3 and S4 demonstrates and supports the unified pattern of the morpHology, with 54% and 76% crystallinity, respectively.

The scattered and aggregated particles, which represent the particles of methylene blue (MB), were seen in all of the loaded samples, and this was followed by a fine modification in their overall morphologies figure 9 (a-d).

The degree of swelling of the four chosen beads was determined at 37^0C and three distinct pH levels are correlated with the morphology of the samples. The biggest holes and caves are seen in S3, which had the greatest degree of swelling (7700 % at pH = 6.8). In contrast, S2 has the lowest swelling (2182% at pH = 6) and does not include any Myrrh in its structure, as well as fractured and uneven surfaces, as explained previously. The remaining two samples, S1 and S4, have a degree of swelling (48625 % and 4286 %, respectively, at pH = 6.8). The presence of Myrrh altered the morphology of the beads and making them more suited to hold water molecules inside their structure and increasing the degree of swelling.

* Corresponding author

Available online at sjuoz.uoz.edu.krd

Science Journal of University of Zakho
Vol. 11, No. 2, pp. 139– 152, April-June 2023

journals.uoz.edu.krd

p-ISSN: 2663-628X
e-ISSN: 2663-6298

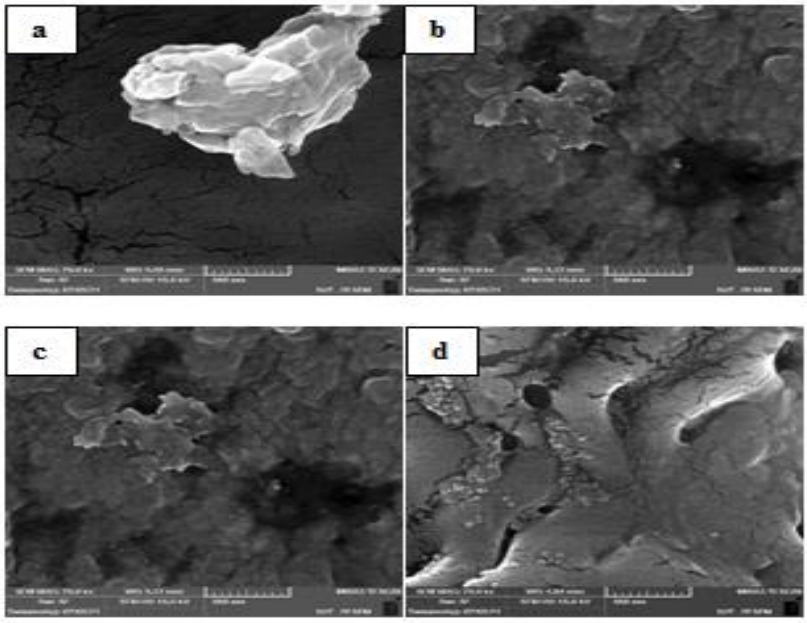

Fig. 9: The SEM images of the four selected Myrrh-Alg loaded beads: a)-S1, b)-S2, c)-S3, d)-S4.

3.5. Physical properties of the composite prepared beads

Table 2 summarizes the physical properties of the Myrrh-Alginate beads. The mean diameters of the Myrrh-Alginate beads tended to rise when the Sodium alginate portion was increased and the presence of Myrrh contributes to this. The proportion of MB in the Myrrh Alginate beads grew considerably as the ratio of Myrrh to Sodium alginate equals or less than two. It was found that the interaction between Myrrh and SA improved the barrier thickness needed to avoid leakage of water from the beads during the processing stage [41]. As a result, drug loss from the beads was minimized.

Table 2: Characteristics of the composite Myrrh- Alginate beads

Samples	Alginate (w/v)	Myrrh (w/v)	Dimeter ofbeads (mm)	Drug content % (w/w)
S1	2.5%	5%	5.5	8.6%
S2	1.75%	0%	3	7.1%
S3	1.5%	9%	4	3.67%
S4	1.5%	0.65%	3	10.3 %

3.6. Swelling Behaviour

The different swelling parameters were estimated through applying the equations as shown below [42-44].
The Mass swelling Ratio (MSR), denoted by Q_t, was estimated using the following equation (vi):

$Q_t\,(MSR) = (M_t - M_0) / M_0$ (vi)

Where M_t = Mass of hydrogel at time (t).
M_0 =Mass of dried hydrogel.

Once the hydrogels reached their maximum weight, several parameters such as the equilibrium swelling ratio (ESR) and equilibrium water content (EWC) were measured by using the equations (vii,viii) below.

$Q_e\,(ESR) = (M_{max} - M_0) / M_0$ (vii)

$EWC = (M_{max} - M_0) / M_{max}$ (viii)

Where: M_{max} is the maximum mass of the hydrogel when it is in equilibrium.
Diffusion is responsible for the movement of water molecules into the polymer network. Hydrogels frequently exhibit swelling properties that correlate to the given mathematical model (ix) [45].

$Q_t / Q_e = kt^n$ (ix)

* Corresponding author

Where: K = Constant of Swelling.
n = The diffusional exponent explains how liquid diffuses into a hydrogel matrix.
t = Swelling-time in minutes.
It is necessary to use the plot of log (Qt/Qe) along the Y-axis as a function of log (t) along the X-axis in order to obtain the appropriate values of k and n away from the intercept and slope of the straight line, respectively.
The following equation can be used to determine the total number of water absorbing-sites (N) in the Hydrogel eq. (x). Where m = 2.99 X 10^{-23} gm which it is the water molecule mass.

$$N = (M_{max} - M_0) / m \qquad (x)$$

As expected, Figure 10 depicts the linear development of log (Qt/Qe) with log (t) for the four taken samples at 37^0C temperatures and two different pH values (pH= 6.8 and 10). The values of n and k were calculated using the slope and intercept of the same plot, as given in tables (4-9) at three temperatures and two pH-levels. Calculating the diffusional exponent, n, provides understanding of the physical mechanism controlling solvent absorption by or medicine releasing from a specific device (Table 3). n = 0.5 denotes Fickian diffusion, n > 0.5 means non-Fickian diffusion, and n = 1 indicates case II (relaxation-controlled) [46].

Table 3: swelling mechanisms and diffusional exponents for hydrogel [47].

Type of transport	Diffusional exponent (n)	Time dependence
Fickian diffusion	0.5	$t^{1/2}$
Anomalous transport	0.5 < n < 1	t^{n-1}
Case II transport	1	Time independent

The overall results demonstrate definitely that the four distinct styles of beads exhibited various swelling methods based on the temperature and pH value of the swelling solution. At pH = 6.8 and at the three distinct temperatures, a non-Fickian diffusional behaviour is observed in addition to that found in (case II). However, the Fickian diffusional behaviour was detected in addition to the other two methods when pH was set to 10.
According to the differences in ESR measurements for each individual sample under varied pH and temperature circumstances, these hydrogels showed a dual sensitivity to pH and temperature Figure (10,11). The ESR results were significantly higher at pH = 6.8, which could be explained by the polymer functional groups becoming suitably ionised table (4-9).
It is significanttaly clear to note that the EWC values are nearly identical and high for the three models prepared with Myrrh as a crosslinker or as included in the core of the synthesised beads whereas the lowest EWC values were observed for the model prepared by dripping pure sodium-alginate in a solution of calcium chloride at various temperatures and sodium alginate ratios.

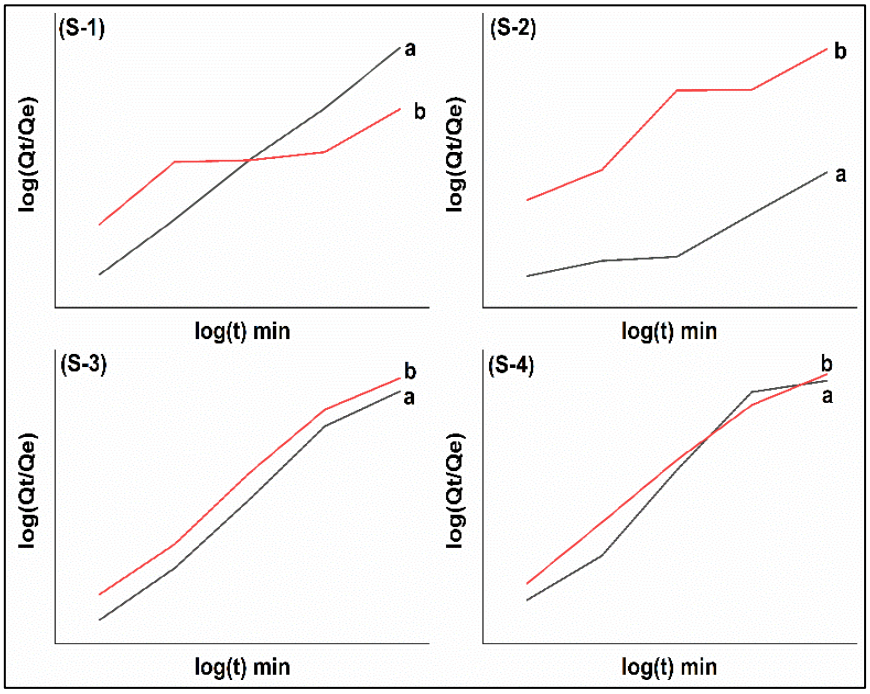

Figure 10: Plot of log (Qt/Qe) against log (t) for four samples at: a) pH = 6.8, b) pH = 10 and 37^0C

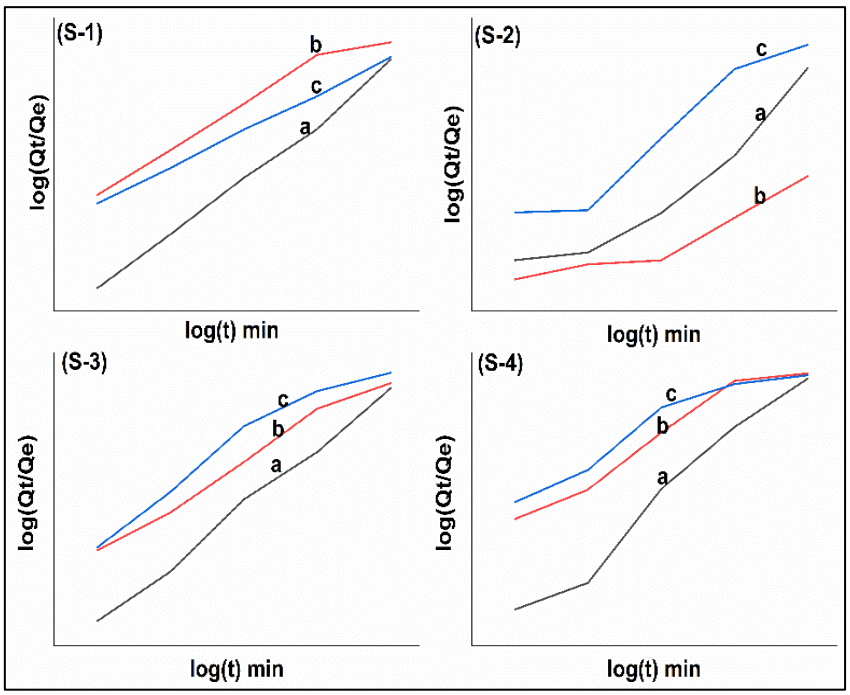

Figure 11: Plot of log (Qt/Qe) against log (t) for four samples at: a) 27 ^{0}C, b) 37 ^{0}C, c) 47 ^{0}C and pH = (6.8).

Table 4: Various swelling parameters of the four selected beads at pH = 6.8 and 27 ^{0}C.

Sample at 27 ^{0}C	M_0 (gm)	M_{Max} (gm)	K	n	ESR	EWC	N * 10^21
1	0.0061	0.476	3.08	1.08	77	0.987	15.7
2	0.0067	0.4325	4.913	1.63	63.55	0.984	15.3
3	0.0055	0.5521	2.775	0.994	99.38	0.99	18.4
4	0.0039	0.3627	5.38	1.994	92	0.989	12

Table 5: Various swelling parameters of the four selected beads at pH = 6.8 and 37 ^{0}C.

Sample at 37 ^{0}C	M_0 (gm)	M_{Max} (gm)	K	n	ESR	EWC	N * 10^21
1	0.0103	0.535	2.015	0.701	51.699	0.98	17.5
2	0.0086	0.1963	3.811	0.861	21.825	0.956	6.26
3	0.006	0.468	2.014	0.744	75.333	0.987	15.4
4	0.0064	0.28	4.396	1.702	42.75	0.977	9.17

Table 6: Various swelling parameters of the four selected beads at pH = 6.8 and 47 ^{0}C.

Sample at 37 ^{0}C	M_0 (gm)	M_{Max} (gm)	K	n	ESR	EWC	N * 10^21
1	0.0103	0.535	2.015	0.701	51.699	0.98	17.5
2	0.0086	0.1963	3.811	0.861	21.825	0.956	6.26
3	0.006	0.468	2.014	0.744	75.333	0.987	15.4
4	0.0064	0.28	4.396	1.702	42.75	0.977	9.17

Table 7: Various swelling parameters of the four selected beads at pH = 10 and 27 ^{0}C.

Sample at 37 ^{0}C	M_0 (gm)	M_{Max} (gm)	K	n	ESR	EWC	N * 10^21
1	0.0103	0.535	2.015	0.701	51.699	0.98	17.5
2	0.0086	0.1963	3.811	0.861	21.825	0.956	6.26
3	0.006	0.468	2.014	0.744	75.333	0.987	15.4
4	0.0064	0.28	4.396	1.702	42.75	0.977	9.17

Table 8: Various swelling parameters of the four selected beads at pH = 10 and 37 ^{0}C.

Sample at 37 ^{0}C	M_0 (gm)	M_{Max} (gm)	K	n	ESR	EWC	N * 10^21
1	0.0103	0.535	2.015	0.701	51.699	0.98	17.5
2	0.0086	0.1963	3.811	0.861	21.825	0.956	6.26
3	0.006	0.468	2.014	0.744	75.333	0.987	15.4
4	0.0064	0.28	4.396	1.702	42.75	0.977	9.17

Table 9: Various swelling parameters of the four selected beads at pH = 10 and 47 ^{0}C.

Sample at 37 ^{0}C	M_0 (gm)	M_{Max} (gm)	K	n	ESR	EWC	N * 10^21
1	0.0103	0.535	2.015	0.701	51.699	0.98	17.5
2	0.0086	0.1963	3.811	0.861	21.825	0.956	6.26
3	0.006	0.468	2.014	0.744	75.333	0.987	15.4
4	0.0064	0.28	4.396	1.702	42.75	0.977	9.17

3.5 Drug Release Kinetics.

Figure 12 shows the amount of drug released as a function of time at various pH values, and the graphs clearly illustrate that a considerable amount of drug is released at all pH values. The maximum amount of medicine is released at pH 10. Up to 99 % of the drug in some synthesised samples is released within the first 24 hours. In comparison to pure calcium alginate, sample two (S2) as shown in Figure 12(b); sample one (S1) and sample four (S4), Figure 12(a,d) display more regulate and controllable releasing behavior at pH = 6.8, confirming the significant effect of Myrrh on the structure and mechanism of the newly synthesised beads.

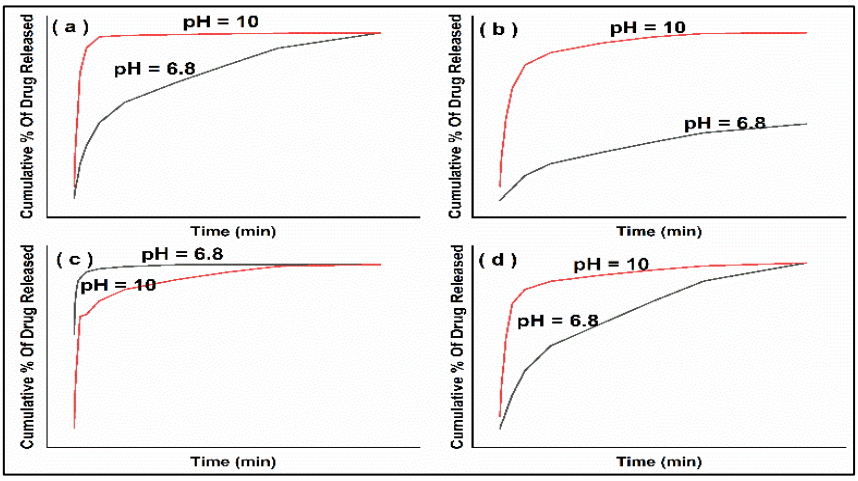

Figure 12: Plots of cumulative % release vs. time at two pH-levels (6.8 and 10) for a)- S1, b)-S2, c)- S3, d)-S4.

After comparing several kinetic models of release profile at two pH levels, the correlation coefficient value seems to be greatest for both the Peppas model and Higuchi at all pH values, as shown in figure 13, 14 and Table 10 (a,b). As a necessary consequence, the Peppas model perfectly represents drug release kinetics throughout all pH levels [48-53].

Table 10 (a): kinetic constants for drug release at pH = 6.8

Sample	Zero order kinetics model		First order kinetics model		Higuchi model		Peppas model		
	K (mol/L)/S	R^2	K 1/S	R^2	K √(mol/L) /S	R^2	K $(mol/L)^{1-n}$ /S	n	R^2
1	0.001	0.88	2.02	0.48	3.75	0.98	0.17	0.78	0.94
2	0.001	0.96	3.07	0.48	4.02	0.98	1.60	1.16	0.97
3	4.96	0.40	0.15	0.25	73.70	0.60	1.77	0.09	0.82
4	0.001	0.95	2.45	0.55	6.78	0.98	0.39	0.80	0.99

Table 10 (b): kinetic constants for drug release at pH = 10.

Sample	Zero order kinetics model		First order kinetics model		Higuchi model		Peppas model		
	K (mol/L)/S	R^2	K 1/S	R^2	K √(mol/L) /S	R^2	K $(mol/L)^{1-n}$ /S	n	R^2
1	2.13	0.33	1.16	0.38	18.68	0.76	0.79	0.51	0.86
2	2.70	0.54	1.42	0.51	9.27	0.91	0.71	0.50	0.94
3	2.25	0.48	1.10	0.36	22.95	0.74	0.93	0.42	0.83
4	2.52	0.49	1.36	0.47	11.61	0.86	0.72	0.51	0.92

The release of MB from S1 and S4 of synthesized hydrogels which contain Myrrh in their structure demonstrates an anomalous kinetic model [53], whereas the release of methylene blue from S2, which is pure calcium alginate, is guided by macromolecular relaxation of the polymer network (Super Case-II transport) at small PH values as well as fickian diffusion [54] at greater PH levels, as seems to be the same with all other samples.

As a result of the low release exponent value (0.5) in this study, Fickian diffusion is observed when the pH level is 10. As a result, drug diffusion occurs at a slower pace than polymer network relaxation. At pH 10, the pore size of a hydrogel reaches its maximum. These findings corroborate those of many additional studies [55,56]. The drug is released more rapidly when the pH climbs from 6 to 10. This effect is explained by an anionically charged carboxylate group in the pH 10 zone. The decrease in drug release at pH 6.8 is due to the presence of a reduced pore size induced by the dissociation of the physical forces between the polymeric chains.

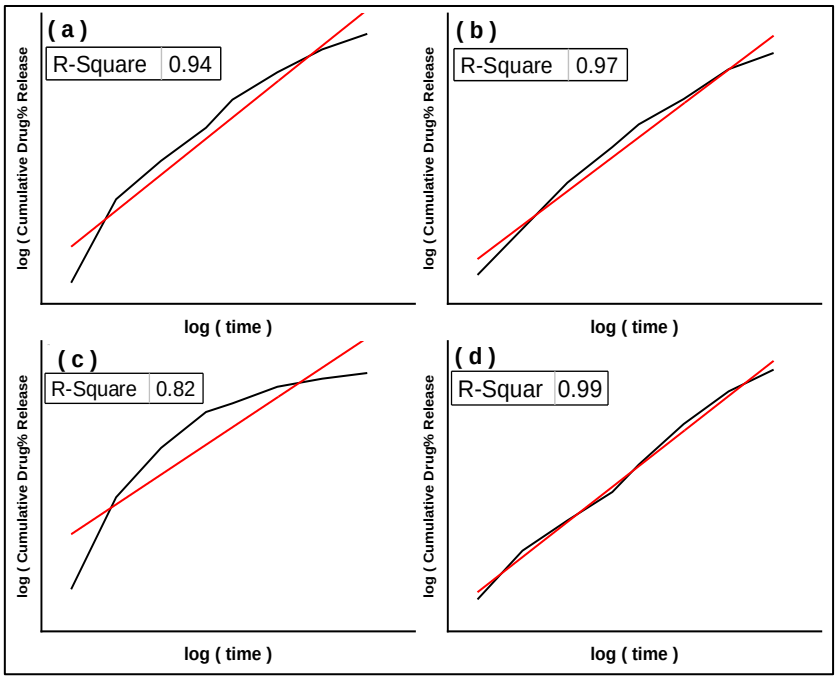

Figure 13: plot log (cumulative % drug release) vis log(time) [Peppas model] at pH = 6.8 and 37ºC for a)- sample-1, b)- sample-2, c)- sample-3, d)- sample-4.

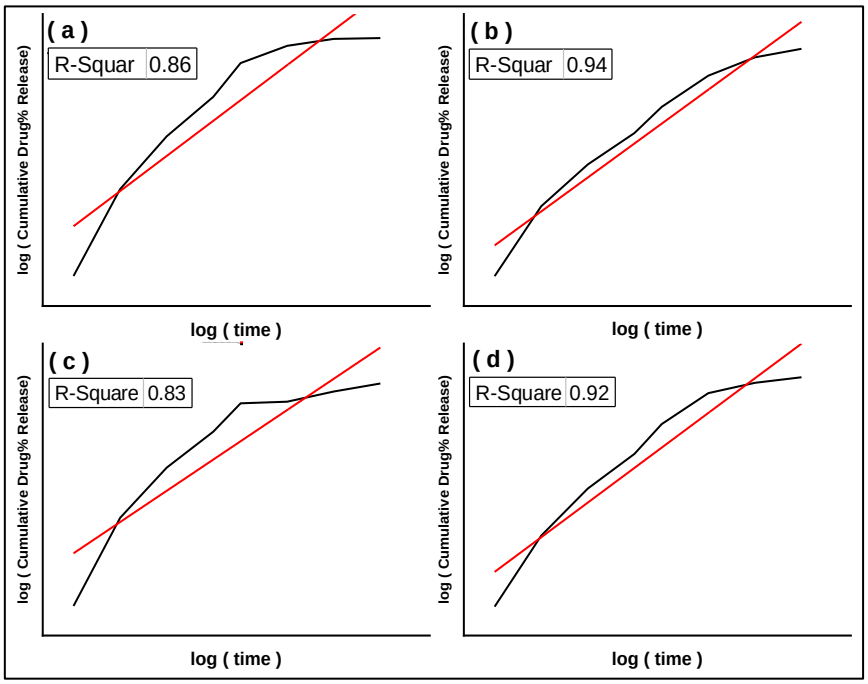

Figure 14: plot log (cumulative % drug release) vis log(time) [Peppas model] at pH = 10 and 37ºC for a)- sample-1, b)- sample-2, c)- sample-3, d)- sample-4.

Conclusion:

The new Eco-friendly composite have prepared through using two natural products (Sodium alginate and Myrrh gum). Myrrh has been used in two ways: a crosslinker as in (S1) and a part of the core mixed with sodium alginate as in (S3, S4). The new green composite models showed an excellent ability to absorb water molecules as they represent higher degree of swelling comparing with pure calcium alginate hydrogel (S2). In addition the models provided different morphological pattern which confirmed through their SEM images. Its worth to mention that the swelling kinetics at two different pH values (6.8 , 10) and three distinct temperatures (27ºC, 37ºC,47ºC) confirmed the dual responsivity (pH-temperature) of the new composite. The drug release kinetic follows Peppas model after using (MB) as drug model and the value of release exponent was (n = 0.5). The results of (FTIR Spectroscopy, XRD, SEM,EDX,TG-DSC) techniques showed that the prepared hydrogel were a suitable candidate for sustained deilevry of drug.

REFERENCES.

Draget, K. I., PHilips, G. O., & Williams, P. A. (2000). Handbook of hydrocolloids.

Sugawara, S., Imai, T., & Otagiri, M. (1994). The controlled release of prednisolone using alginate gel. PHarmaceutical Research, 11(2), 272-277.

Hwang, S. J., Rhee, G. J., Lee, K. M., Oh, K. H., & Kim, C. K. (1995). Release characteristics of ibuprofen from excipient-loaded alginate gel beads. International journal of pHarmaceutics, 116(1), 125-128.

Fernandez-Hervas, M. J., Holgado, M. A., Fini, A., & Fell, J. T. (1998). In vitro evaluation of alginate beads of a diclofenac salt. International Journal of PHarmaceutics, 163(1-2), 23-34.

Kikuchi, A., Kawabuchi, M., Sugihara, M., Sakurai, Y., & Okano, T. (1997). Pulsed dextran release from calcium-alginate gel beads. Journal of Controlled Release, 47(1), 21-29.

Grant, G. T. (1973). Biological interactions between polysaccharides and divalent cations: the egg-box model. Febs Lett., 32, 195-198.

Kim, M. S., Park, G. D., Jun, S. W., Lee, S., Park, J. S., & Hwang, S. J. (2005). Controlled release tamsulosin hydrochloride from alginate beads with waxy materials. Journal of PHarmacy and Pharmacology, 57(12), 1521-1528.

Pongjanyakul, T., Sungthongjeen, S., & Puttipipatkhachorn, S. (2006). Modulation of drug release from glyceryl palmitostearate–alginate beads via heat treatment. International journal of pharmaceutics, 319(1-2), 20-28.

Puttipipatkhachorn, S., Pongjanyakul, T., & Priprem, A. (2005). Molecular interaction in alginate beads reinforced with sodium starch glycolate or magnesium aluminum silicate, and their pHysical characteristics. International journal of pHarmaceutics, 293(1-2), 51-62.

Murata, Y., Tsumoto, K., Kofuji, K., & Kawashima, S. (2003). Effects of natural polysaccharide addition on drug

release from calcium-induced alginate gel beads. Chemical and pHarmaceutical bulletin, 51(2), 218-220.

Murata, Y., Miyamoto, E., & Kawashima, S. (1996). Additive effect of chondroitin sulfate and chitosan on drug release from calcium-induced alginate gel beads. Journal of controlled release, 38(2-3), 101-108.

Ammar, C., El Ghoul, Y., & El Achari, A. (2015). Finishing of polypropylene fibers with cyclodextrins and polyacrylic acid as a crosslinking agent. Textile Research Journal, 85(2), 171-179.

Hanuš, L. O., Řezanka, T., Dembitsky, V. M., & Moussaieff, A. (2005). Myrrh-commipHora chemistry. Biomedical papers, 149(1), 3-28.

Greve, H. L., Kaiser, M., & Schmidt, T. J. (2020). Investigation of antiplasmodial effects of terpenoid compounds isolated from Myrrh. Planta medica, 86(09), 643-654.

Hough, L., Jones, J. K. N., & Wadman, W. H. (1952). 144. Some observations on the constitution of gum Myrrh. Journal of the Chemical Society (Resumed), 796-800.

Langhorst, J., Varnhagen, I., Schneider, S. B., Albrecht, U., Rueffer, A., Stange, R., ... & Dobos, G. J. (2013). Randomised clinical trial: a herbal preparation of Myrrh, chamomile and coffee charcoal compared with mesalazine in maintaining remission in ulcerative colitis–a double-blind, double-dummy study. Alimentary pHarmacology & therapeutics, 38(5), 490-500.

Shen, T., Li, G. H., Wang, X. N., & Lou, H. X. (2012). The genus CommipHora: a review of its traditional uses, pHytochemistry and pHarmacology. Journal of ethnopHarmacology, 142(2), 319-330.

Ahamad, S. R., Al-Ghadeer, A. R., Ali, R., Qamar, W., & Aljarboa, S. (2017). Analysis of inorganic and organic constituents of Myrrh resin by GC–MS and ICP-MS: An empHasis on medicinal assets. Saudi PHarmaceutical Journal, 25(5), 788-794.

Agrawal, A., & Purwar, R. (2018). Swelling and drug release kinetics of composite wound dressing. Indian Journal of Fibre & Textile Research (IJFTR), 43(1), 104-111.

Adnadjevic, B., & Jovanovic, J. (2009). A comparative kinetics study of isothermal drug release from poly (acrylic acid) and poly (acrylic-co-methacrylic acid) hydrogels. Colloids and Surfaces B: Biointerfaces, 69(1), 31-42.

Martinez-Ruvalcaba, A., Sánchez-Díaz, J. C., Becerra, F., Cruz-Barba, L. E., & Gonzalez-Alvarez, A. (2009). Swelling characterization and drug delivery kinetics of polyacrylamide-co-itaconic acid/chitosan hydrogels. Express Polym Lett, 3(1), 25-32.

Thakur, A., Wanchoo, R. K., & Singh, P. (2011). Hydrogels of poly (acrylamide-co-acrylic acid): in-vitro study on release of gentamicin sulfate. Chemical and Biochemical Engineering Quarterly, 25(4), 471-482.

Katime, I., Novoa, R., de Apodaca, E. D., Mendizábal, E., & Puig, J. (1999). TheopHylline release from poly (acrylic acid-co-acrylamide) hydrogels. Polymer Testing, 18(7), 559-566.

Serra, L., Doménech, J., & Peppas, N. A. (2006). Drug transport mechanisms and release kinetics from molecularly designed poly (acrylic acid-g-ethylene glycol) hydrogels. Biomaterials, 27(31), 5440-5451.

Jovanovic, J., Adnadjevic, B., & Kostic, A. (2010). The effects of the pH value of the swelling medium on the kinetics of the swelling of a poly (acrylic acid) hydrogel. Journal of applied polymer science, 116(2), 1036-1043.

Manuja, A., Kumar, S., Dilbaghi, N., Bhanjana, G., Chopra, M., Kaur, H., ... & Yadav, S. C. (2014). Quinapyramine sulfate-loaded sodium alginate nanoparticles show enhanced trypanocidal activity. Nanomedicine, 9(11), 1625-1634.

Yeom, C. K., & Lee, K. H. (1998). Characterization of sodium alginate membrane crosslinked with glutaraldehyde in pervaporation separation. Journal of applied polymer science, 67(2), 209-219.

Cardenas-Jiron, G., Leal, D., Matsuhiro, B., & Osorio-Roman, I. O. (2011). Vibrational spectroscopy and density functional theory calculations of poly-D-mannuronate and heteropolymeric fractions from sodium alginate. Journal of Raman Spectroscopy, 42(4), 870-878.

Chandıa, N. P., Matsuhiro, B., & Vásquez, A. E. (2001). Alginic acids in Lessonia trabeculata: characterization by formic acid hydrolysis and FT-IR spectroscopy. Carbohydrate Polymers, 46(1), 81-87.

Daemi, H., & Barikani, M. (2012). Synthesis and characterization of calcium alginate nanoparticles, sodium homopolymannuronate salt and its calcium nanoparticles. Scientia Iranica, 19(6), 2023-2028.

Benhouria, A., Islam, M. A., Zaghouane-Boudiaf, H., Boutahala, M., & Hameed, B. H. (2015). Calcium alginate–bentonite–activated carbon composite beads as highly effective adsorbent for MB. Chemical engineering journal, 270, 621-630.

Li, Z., Yao, Y., Wei, G., Jiang, W., Wang, Y., & Zhang, L. (2016). Adsorption and heat-energy-aid desorption of cationic dye on a new thermo-sensitive adsorbent: Methyl cellulose/calcium alginate beads. Polymer Engineering & Science, 56(12), 1382-1389.

Li, M., Han, G., & Yu, J. (2010). Microstructure and mechanical properties of apocynum venetum fibers extracted by alkali-assisted ultrasound with different frequencies. Fibers and Polymers, 11(1), 48-53.

Ricciardi, R., Auriemma, F., De Rosa, C., & Lauprêtre, F. (2004). X-ray diffraction analysis of poly (vinyl alcohol) hydrogels, obtained by freezing and thawing techniques. Macromolecules, 37(5), 1921-1927.

Yang, G., Zhang, L., Peng, T., & Zhong, W. (2000). Effects of Ca2+ bridge cross-linking on structure and pervaporation of cellulose/alginate blend

membranes. Journal of Membrane Science, 175(1), 53-60.

Gaur, S., & Reed, T. B. (2020). Thermal data for natural and synthetic fuels. CRC press.

Kato, K. (1953). THERMAL DECOMPOSITION OF ALGINS: AS DETERMINED BY THERMO-BALANCE METHOD. Faculty of Fesheries Hokkaido University, 4(1), 40-42.

Farmoudeh, A., Akbari, J., Saeedi, M., Ghasemi, M., Asemi, N., & Nokhodchi, A. (2020). Methylene blue-loaded niosome: preparation, pHysicochemical characterization, and in vivo wound healing assessment. Drug delivery and translational research, 10(5), 1428-1441.

Rager, T., Geoffroy, A., Hilfiker, R., & Storey, J. M. (2012). The crystalline state of methylene blue: a zoo of hydrates. PHysical Chemistry Chemical PHysics, 14(22), 8074-8082.

Pasparakis, G., & Bouropoulos, N. (2006). Swelling studies and in vitro release of verapamil from calcium alginate and calcium alginate–chitosan beads. International journal of pHarmaceutics, 323(1-2), 34-42.

Dashevsky, A. (1998). Protein loss by the microencapsulation of an enzyme (lactase) in alginate beads. International journal of PHarmaceutics, 161(1), 1-5.

Barati, A. (2010). Swelling kinetics modeling of cationicmethacrylamide-based hydrogels. World Appl. Sci. J., 11, 1336-1341.

KARADAĞ, E., & Saraydin, D. U. R. S. U. N. (2002). Swelling of superabsorbent acrylamide/sodium acrylate hydrogels prepared using multifunctional crosslinkers. Turkish Journal of Chemistry, 26(6), 863-876.

Kim, S. J., Park, S. J., & Kim, S. I. (2003). Synthesis and characteristics of interpenetrating polymer network hydrogels composed of poly (vinyl alcohol) and poly (N-isopropylacrylamide). Reactive and Functional Polymers, 55(1), 61-67.

Ganji, F., Vasheghani, F. S., & VASHEGHANI, F. E. (2010). Theoretical description of hydrogel swelling: a review.

Gouda, R., Baishya, H., & Qing, Z. (2017). Application of mathematical models in drug release kinetics of carbidopa and levodopa ER tablets. J. Dev. Drugs, 6(02), 1-8.

Vigata, M., Meinert, C., Pahoff, S., Bock, N., & Hutmacher, D. W. (2020). Gelatin methacryloyl hydrogels control the localized delivery of albumin-bound paclitaxel. Polymers, 12(2), 501.

Qureshi, D., Nayak, S. K., Maji, S., Anis, A., Kim, D., & Pal, K. (2019). Environment sensitive hydrogels for drug delivery applications. European Polymer Journal, 120, 109220.

Dash, S., Murthy, P. N., Nath, L., & Chowdhury, P. (2010). Kinetic modeling on drug release from controlled drug delivery systems. Acta Pol PHarm, 67(3), 217-223.

Korsmeyer, R. W., Gurny, R., Doelker, E., Buri, P., & Peppas, N. A. (1983). Mechanisms of solute release from porous hydropHilic polymers. International journal of pHarmaceutics, 15(1), 25-35.

Ritger, P. L., & Peppas, N. A. (1987). A simple equation for description of solute release II. Fickian and anomalous release from swellable devices. Journal of controlled release, 5(1), 37-42.

Siepmann, J., & Peppas, N. A. (2012). Modeling of drug release from delivery systems based on hydroxypropyl methylcellulose (HPMC). Advanced drug delivery reviews, 64, 163-174.

Katime, I., & Mendizábal, E. (2010). Swelling properties of new hydrogels based on the dimethyl amino ethyl acrylate methyl chloride quaternary salt with acrylic acid and 2-methylene butane-1, 4-dioic acid monomers in aqueous solutions. Mater Sci Appl, 1(3), 162-7.

Thakur, A., Wanchoo, R. K., & Singh, P. (2011). Structural parameters and swelling behavior of pH sensitive poly (acrylamide-co-acrylic acid) hydrogels. Chemical and Biochemical Engineering Quarterly, 25(2), 181-194.

Peppas, N. A., & Khare, A. R. (1993). Preparation, structure and diffusional behavior of hydrogels in controlled release. Advanced drug delivery reviews, 11(1-2), 1-35.

Jovanovic, J., Adnadjevic, B., & Kostic, A. (2010). The effects of the pH value of the swelling medium on the kinetics of the swelling of a poly (acrylic acid) hydrogel. Journal of applied polymer science, 116(2), 1036-1043.